Electrocatalysis (2015) 6:398–404
DOI 10.1007/s12678-015-0260-3

ORIGINAL RESEARCH

Structure and Surface Reactivity of Ultra-Thin Pt/W(111) Films

Mohammad K. El Jawad[1,2,3,4] · **Bruno Gilles**[3,4] · **Frédéric Maillard**[1,2]

Published online: 19 May 2015

Abstract We report on the structure, the chemisorption and the electrocatalytic properties of multilayer (2.2, 3.3 and 5.5 physical monolayers) Pt films deposited on W(111) elaborated by molecular beam epitaxy. The Pt/W(111) surfaces were characterized by low-energy electron diffraction (LEED), X-ray photoelectron spectroscopy (XPS) and cyclic voltammetry (CV). Pronounced changes of the surface reactivity were noticed as the Pt coverage is decreased. In particular, the affinity for under-potentially deposited hydrogen (H_{upd}) and hydroxyl (OH_{ads}) species and the ability to electrooxidize a monolayer of CO_{ads} were depreciated in agreement with strain and ligand effects.

Keywords Molecular beam epitaxy · Single crystals · Platinum · Strain effect · Ligand effect

Introduction

The chemisorption and catalytic properties of a metal surface depend on its electronic [1, 2] and structural properties [3–5]. In that respect, bimetallic surfaces attract tremendous research interest because they offer the opportunity to tailor the selectivity, the catalytic activity and the stability of a given metal. Besides 'ensemble effects' [6], the modifications of the catalytic properties of a bimetallic surface are attributed to the combination of strain and ligand effects [7–16]. The strain effect arises from the compressed or expanded arrangement of the surface metal atoms and consequently increases or decreases the width of the electronic bands of the surface metal atoms. Expanding the lattice of the surface atoms leads to smaller atomic orbital overlap and thus reduces the width of the *d*-band. If the *d*-band is more than half filled, charge conservation causes an upshift of the *d*-band centre closer to the Fermi level and increases the surface reactivity. On the contrary, a compressed lattice makes the surface atoms less reactive due to the downshift of the *d*-band centre away from the Fermi level. The ligand effect is due to the change in the chemical properties of the metal surface atoms by the neighbouring element and causes similar variation of the chemisorption properties. Decoupling the strain and ligand effect is hardly feasible experimentally. An elegant approach by Gsell et al. [17] consisted of producing local strain on a Ru(0001) single crystal by means of subsurface gas bubbles resulting from Ar^+ ion sputtering and annealing at moderate temperature (T ~1000 K). The Ru lattice was submitted to a tensile strain close to the top part of the bubbles, while the periphery of the regions was subjected to compressive strain. Oxygen molecules were found to adsorb preferentially on local areas of the surface with expanded lattice (tensile strain) [17]. Surface strain may also be applied by using metal films grown on single crystals [15, 16, 18]. In case of small lattice mismatch between the metal surface atoms and the underlying substrate, the surface atoms are deposited pseudomorphically with a lattice constant nearly identical to the substrate material. If the lattice mismatch is large, the deposited film relaxes and grows with its own lattice parameter upon a certain film thickness [19]. Thus, by varying the film thickness or the film–

✉ Bruno Gilles
bruno.gilles@simap.grenoble-inp.fr

✉ Frédéric Maillard
frederic.maillard@lepmi.grenoble-inp.fr

[1] Univ. Grenoble Alpes, LEPMI, 38000 Grenoble, France

[2] CNRS, LEPMI, 38000 Grenoble, France

[3] Univ. Grenoble Alpes, SIMAP, 38000 Grenoble, France

[4] CNRS, SIMAP, 38000 Grenoble, France

substrate pair, different systems with varied amounts of tensile or compressive strain can be obtained. Using this approach, Kibler et al. [15, 16] tailored the electrocatalytic activity of Pd atoms for the electrooxidation of formic acid. Hoster et al. [20] showed that the affinity to hydrogen atoms (H_{ads}) and hydroxyl species (OH_{ads}) of Pt atoms deposited onto Ru(0001) increases with an increase in the Pt film thickness (i.e. a released compressive strain). This was reflected in cyclic voltammograms by a positive shift of the reversible adsorption of under-potentially deposited H (H_{upd}) and by a negative shift of the OH_{ads} adsorption features. Using a Cu(111) single crystal modified by thin Pt films, Strasser et al. [18] demonstrated that dealloyed Pt-Cu nanoparticles feature enhanced oxygen reduction reaction kinetics because of changes in the electronic structure of Pt due to lateral strain.

In this paper, thin Pt/W(111) films with coverage of 2.2, 3.3 and 5.5 physical monolayers (PMLs) were prepared by molecular beam epitaxy (MBE) and characterized by low-energy electron diffraction (LEED) and X-ray photoelectron spectroscopy (XPS). W(111) is a body-centred cubic surface that is atomically rough and open. As shown by Fig. 1, three outermost layers are exposed to the surface: these three layers form one PML. The surface reactivity of the Pt/W(111) thin films was tested for the adsorption/desorption of under-potentially deposited hydrogen and oxygen (OH species) and for the electrooxidation of a CO_{ads} monolayer.

Experimental Section

The molecular beam epitaxy (MBE) system used to deposit the Pt films was composed of a characterization chamber and a deposition chamber. The characterization chamber was equipped with surface preparation (Ar^+ ion bombardment) and characterization (XPS and LEED) facilities. The substrate holder was a modified Riber 1″ molyblock onto which the single crystal was tightened using tantalum wires. A furnace capable of flash annealing the single crystal at temperatures T>2273 K was positioned at a distance of 1 mm behind the sample. The W(111) single crystal was purchased from Mateck GmbH (99, 999 at%, 0.786 cm^2 geometric). It was oriented and polished to within 0.1° of the (111) crystallographic orientation. The W(111) surface was prepared by several cycles composed of Ar^+ ion bombardment at an energy of 600 eV followed by rapid annealing at T ~2300 K. The annealing of the W(111) single crystal induced surface segregation of chemical impurities such as carbon and oxygen contained in the bulk of the material. These contaminants were removed by Ar^+ bombardment. After each cycle, the structural order was examined by LEED until the diagram showed a hexagonal (1×1) pattern with extinction of only a few spots (Fig. 2).

These extinctions were attributed to a slight residual contamination of the surface with oxygen (typically 0.1 monolayer) and quantified by XPS (Fig. 3).

Pt was evaporated from an electron beam evaporator at a deposition rate of 0.1 Å s^{-1}. The Pt film thickness was measured with a quartz balance, while maintaining the substrate at T ~600 K. Three samples with Pt physical coverages of 2.2, 3.3 and 5.5 PML corresponding to a Pt film thickness of 0.6, 0.8 and 1.3 nm, respectively, were prepared. A home-made transfer chamber enabled the transfer of the Pt/W(111) surfaces from UHV to ambient pressure for electrochemical measurements and transfer back to UHV for chemical and structural analysis (see Ref. [21]). To that goal, the transfer chamber was first disconnected from the main UHV chamber by closing the gate valve and then filled with argon (>99.999 %, referred to as 5 N Ar in what follows) up to the atmospheric pressure. Subsequently, an electrochemical reaction cell made of polychlorotrifluoroethylene (PCTFE) was mounted on top of a metallic tube, moved up into the transfer chamber through an opened gate valve and brought into contact with the as-prepared surface. The model Pt/W(111) electrode was pressed onto an O-ring (Kalrez™6375, Dupont de Nemours) by a mobile rod controlled by a micrometre screw, which also provided direct electrical contact to the sample/sample holder. The O-rings used to seal the electrochemical cell were cleaned by mild boiling into concentrated H_2SO_4/H_2O_2 and

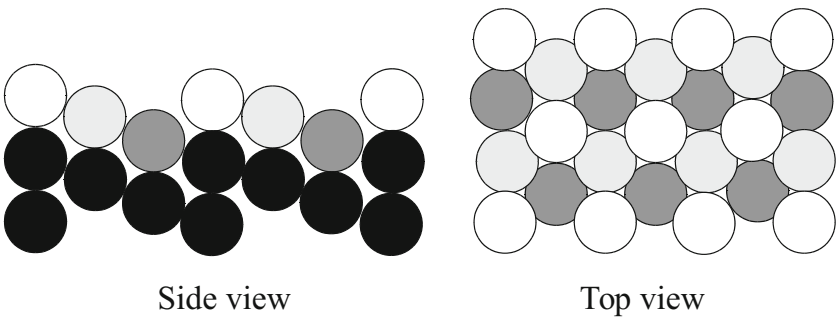

Fig. 1 Top and side view of W(111) surface demonstrates that atoms from the three outermost layers are exposed to the surface—these three atomic layers together form one physical monolayer (PML). The top layer is shown in *white*, the layer beneath is shown in *light grey* and the bottom layer is shown in *grey*

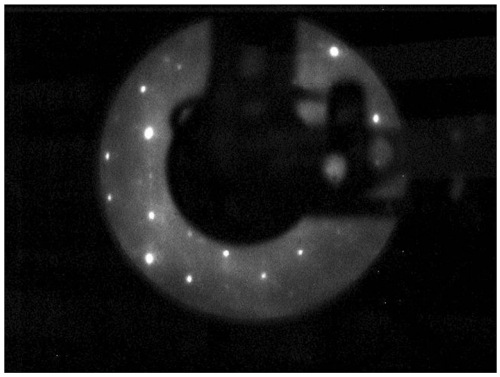

Fig. 2 LEED diagram of a W(111) surface. The energy of the electron beam was 222 eV

thoroughly rinsed in Milli-Q water before their use. The electrochemical experiments were conducted at room temperature using an Autolab/PGSTAT12 potentiostat. The geometric area of the Pt/W(111) single crystal in contact with the electrolyte was 0.5 cm^2. The counter-electrode was a Pt foil and the reference electrode was a freshly prepared reversible hydrogen electrode (RHE). Sulphuric acid (H_2SO_4—Suprapur, Merck) diluted with Milli-Q water to 0.1 M was used as electrolyte solution. Electrolyte purged with argon (5 N Ar) was introduced in the electrochemical cell while maintaining the electrode potential at E=0.1 V vs. RHE. In CO_{ads} stripping experiments, CO molecules were adsorbed by bubbling with CO the electrolyte contained in an Erlenmeyer tank for 20 min and circulating the saturated electrolyte with the help of a peristaltic pump while holding the potential of the working electrode at E=0.1 V vs. RHE. Next, the electrolyte was purged with Ar for 30 min before stripping off the adsorbed CO monolayer during a positive potential sweep at a potential sweep rate of v=0.02 V s^{-1}. After electrochemical experiments, the working electrode was transferred back to UHV for chemical characterization by XPS.

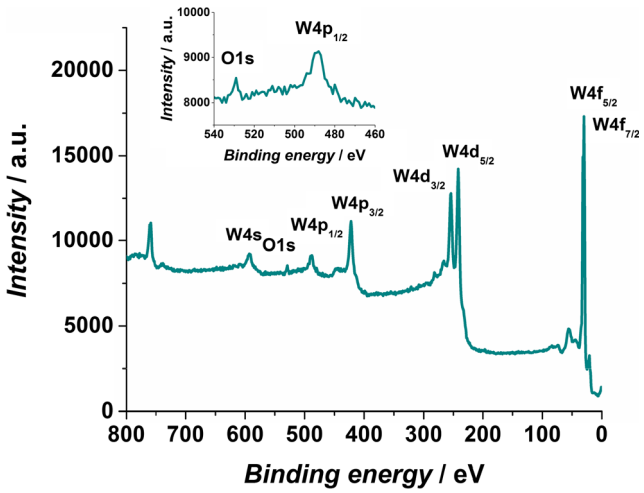

Fig. 3 XPS spectrum of the W(111) surface after several Ar^+ ion bombardment/annealing cycles. The peak observed at 532 eV corresponds to a slight contamination with oxygen (*O1s*)

Results and Discussion

Structural Characterization of the Pt/W(111) Surfaces

Since the Pt atoms feature larger Wigner–Seitz radius than the W atoms [12] and because they possess different structure and lattice parameters,[1] they are under strong compressive strain. For example, if the Pt atoms accommodate with W atoms along the [−2 1 1] direction, the lattice parameter of Pt is contracted by ca 6.8 %. According to the elasticity theory, part of this strain may be relaxed by introducing misfit dislocations above a critical Pt film thickness (h_c). This critical thickness for the Pt/W(111) system was calculated using the Matthews formulation [22, 23]:

$$h_c = \frac{b\left[1-\nu_d\cos^2\theta\right]}{8\pi\pi(1+\nu_d)\varepsilon\varepsilon\cos\lambda}\ln\left(\frac{2h_c}{r_0}\right) + \frac{b(1-\cos^2\theta)}{16\pi6\pi(1+\nu_d)\varepsilon\varepsilon\cos\lambda}\left[\cos2\lambda-\frac{1-2\nu_d}{2(1-\nu_d)}\right] \quad (1)$$

where b is the Burgers vector, θ and λ are two angles of the slip plane and the Burgers vector with respect to the surface, respectively, ν_d is the Poisson ratio's (0.39 for Pt), ε is the lattice misfit and r_0 is related to the cut-off radius of the dislocation and its core energy (frequently r_0=b/2 is used).

Two possible slip systems across 3{111} planes exist for the Pt/W(111) system [24]. The first system corresponds to partial dislocations with a Burgers vector $\vec{b} = \frac{1}{6}[211]$ {111}, while the second corresponds to perfect dislocations with a Burgers vector $\vec{b} = \frac{1}{2}[011]$ {111}. Using Eq. 1, two critical Pt film thicknesses were determined (h_c=0.3 nm for $\vec{b} = \frac{1}{6}$ [211] {111} and h_c=0.5 nm for $\vec{b} = \frac{1}{2}[011]$ {111}). Figure 4 shows that, whatever the slip system considered, misfit dislocations are created in the deposited Pt film after the completion of the first monolayer. These partial dislocations are energetically favourable up to a Pt film thickness h=0.9 nm above which perfect dislocations become energetically more favourable. In each case, Pt atoms supported on W(111) remain compressed by ca 4 to 6 %.

Surface Reactivity of the Pt/W(111) Films

Figure 5a displays the cyclic voltammograms of the $Pt_{2.2PML}$/W(111) surface before and after three CO_{ads} stripping

[1] Bulk W crystallizes in body centred cubic (bcc) structure with a lattice parameter equal to 0.3165 nm, while Pt adopts the face centred cubic (fcc) structure with a lattice parameter equal to 0.3924 nm.

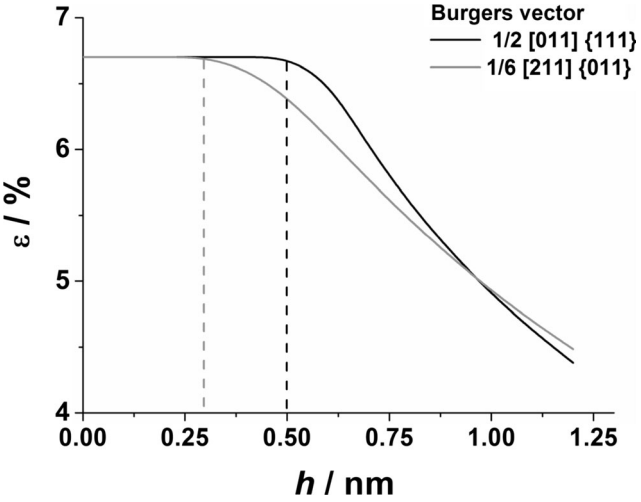

Fig. 4 Relaxation curves obtained for a thin Pt film deposited onto a W(111) surface calculated for the two possible slip systems: $\vec{b} = \frac{1}{6}[211]\ \{111\}$ or $\vec{b} = \frac{1}{2}[011]\ \{111\}$. The *dashed lines* indicate the values of the critical thickness above which misfit dislocations become thermodynamically favourable

experiments in 0.1 M H_2SO_4. On the as-prepared surface, the adsorption-desorption of H_{upd} proceeds via a single broad peak. After the electrochemical experiments, two broad peaks (oxidation region) and a single peak centred at E=0.20 V vs. RHE (reduction region) are observed.

These electrochemical features are very similar to those observed on Pt/WO_3 surfaces with low Pt geometrical coverage (ca 10 %) by Jayaraman et al. [25] and Micoud et al. [26, 27] and suggest an incomplete coverage of the W(111) surface by Pt atoms. In these studies, the oxidation/reduction peaks were assigned to the intercalation/de-intercalation of tungsten bronzes according to the following reaction:

$$WO_3 + yH^+ + ye^- \leftrightarrow H_yWO_3 \quad (2)$$

According to the Pourbaix diagram [28], exposure of the W atoms to acidic environment in the potential range 0.05<E< 0.95 V vs. RHE results in the formation of WO_3. This was confirmed by XPS spectra acquired after the electrochemical measurements (Fig. 6): the W $4f_{7/2}$ and $4f_{5/2}$ transition peaks were observed at 30.7 and 32.7 eV for the fresh $Pt_{\sim 2.2PML}$/W(111) surface and at 35.4 and 37.6 eV after the electrochemical measurements, respectively. Furthermore, the disappearance of the Pt transition peaks indicates that the Pt atoms were

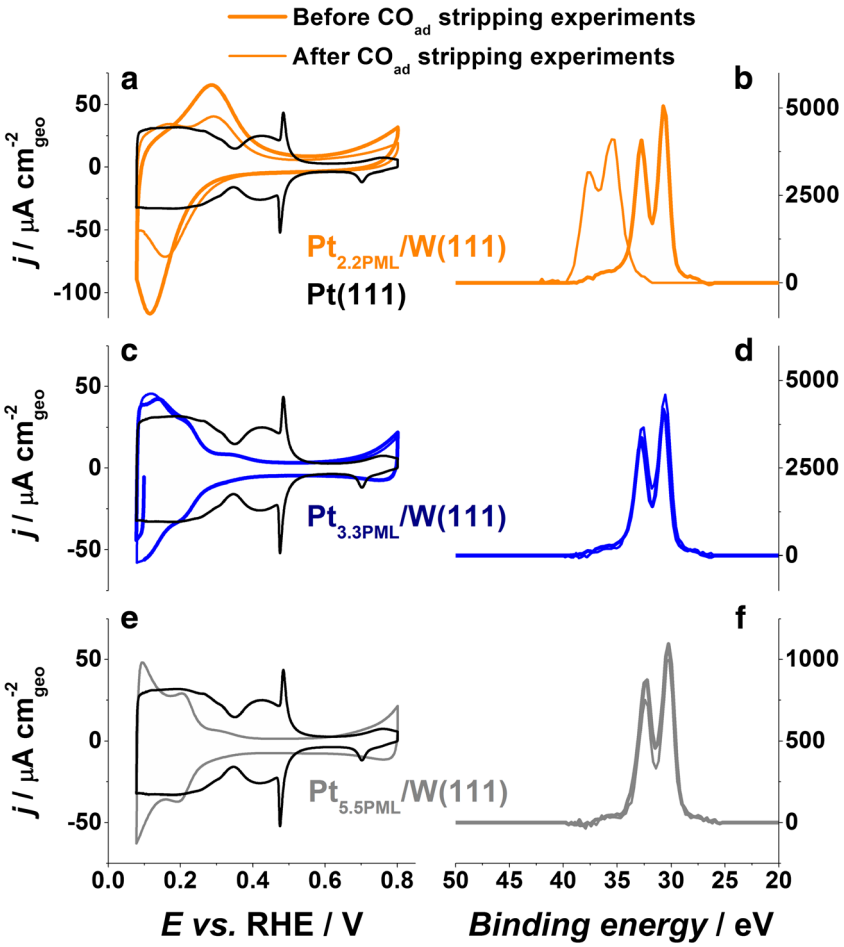

Fig. 5 Cyclic voltammograms (**a**, **c**, **e**) and X-ray photon electron spectra (**b**, **d**, **f**) of $Pt_{x\text{-}PML}$/W(111) (x=2.2, 3.3, 5.5 PML, respectively) recorded before and after three CO_{ads} stripping experiments in 0.1 M H_2SO_4 at a potential sweep rate v= 0.05 V s^{-1}. For the sake of comparison, the cyclic voltammogram of a Pt(111) surface prepared in ultra-high vacuum and transferred to 0.1 M H_2SO_4 is displayed as a *black trace*

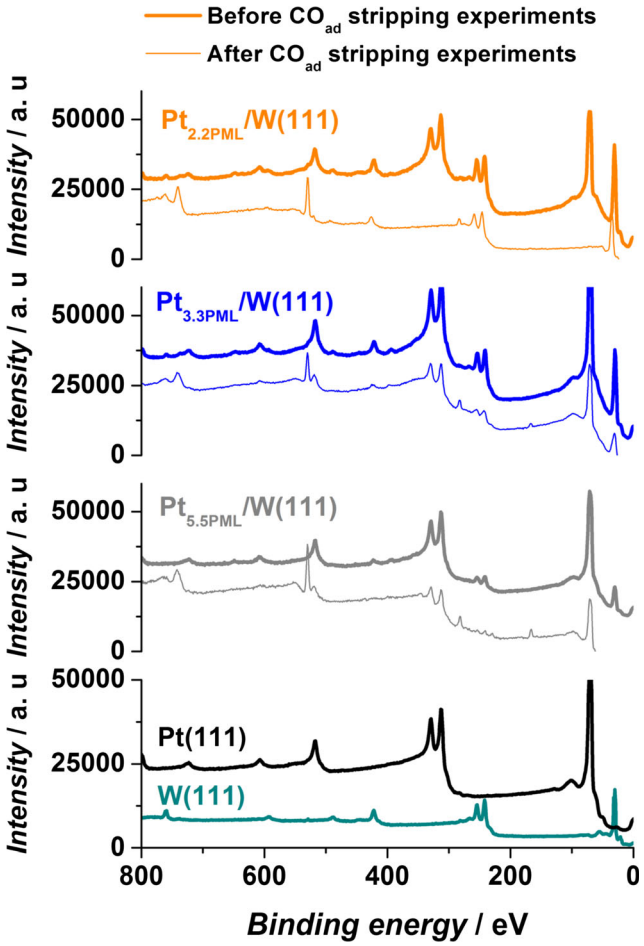

Fig. 6 X-ray photoelectron spectra of the catalytic surfaces evaluated in this work

removed during the electrochemical measurements, most likely as a result of the oxidation of the underlying W atoms.

On $Pt_{3.3\text{-}PML}/W(111)$ and $Pt_{5.5\text{-}PML}/W(111)$, the H_{upd} adsorption/desorption features are typical of a compressed (111) surface (see, for example, the voltammogram of a $Pt_3Ni(111)$ in reference [29]), and remain stable over time (Fig. 5). The W $4f_{7/2}$ and W $4f_{5/2}$ transition peaks measured on the as-prepared $Pt_{3.3\text{-}PML}/W(111)$ and the $Pt_{5.5\text{-}PML}/W(111)$ surfaces are located at 30.7 and 32.7 eV, in agreement with the theoretical values of metallic tungsten [30]. No shift in the XPS peak position after the electrochemical experiments discards the possibility of W oxides or Pt–W alloy formation (Fig. 5d). In addition, the ratio of the intensity of the Pt and the W transition peaks remained nearly constant before/after the electrochemical experiments, therefore excluding the desorption of Pt atoms from the W(111) surface.

A 100-mV shift of the H_{upd} adsorption/desorption region towards negative potentials is observed with decreasing Pt film thicknesses (i.e. increasing compressive strain, Fig. 5c, e). This result agrees with the *d*-band theory [11, 31] and former experimental observations of Hoster et al. [20] on Pt/Ru(0001) and Van der Vliet et al. on a $Pt_3Ni(111)$-skin surface [29]. According to Pallassana et al. [31], this shift in potential may be rationalized by considering that changes of the chemisorption energy of hydrogen atoms depend on the *d*-band centre of the surface metal atoms as

$$\delta E_{chem} = \frac{V^2}{(\Delta\Delta\varepsilon)^2}\delta\varepsilon_d \tag{3}$$

where V^2 is the *d*-band coupling matrix element for the surface metal atom and $\Delta\varepsilon=|\varepsilon_d-\varepsilon_a|$ the difference between ε_d and ε_a, the location of the *d*-band centre and the H1*s* orbital state, respectively.

CO_{ads} Stripping Experiments

The CO_{ads} monolayer electrooxidation follows a Langmuir–Hinshelwood mechanism, where OH_{ads} is formed by water splitting; CO_{ads} + OH_{ads} recombine on two adjacent sites to form $COOH_{ads}$, which ultimately is oxidized into CO_2:

$$H_2O + Pt \leftrightarrow Pt\text{–}OH_{ads} + H^+ + e^- \tag{4}$$

$$CO_{ads} + OH_{ads} \rightarrow COOH_{ads} \tag{5}$$

$$COOH_{ads} \rightarrow CO_2 + H^+ + e^- + 2* \tag{6}$$

where * denotes a free Pt surface site.

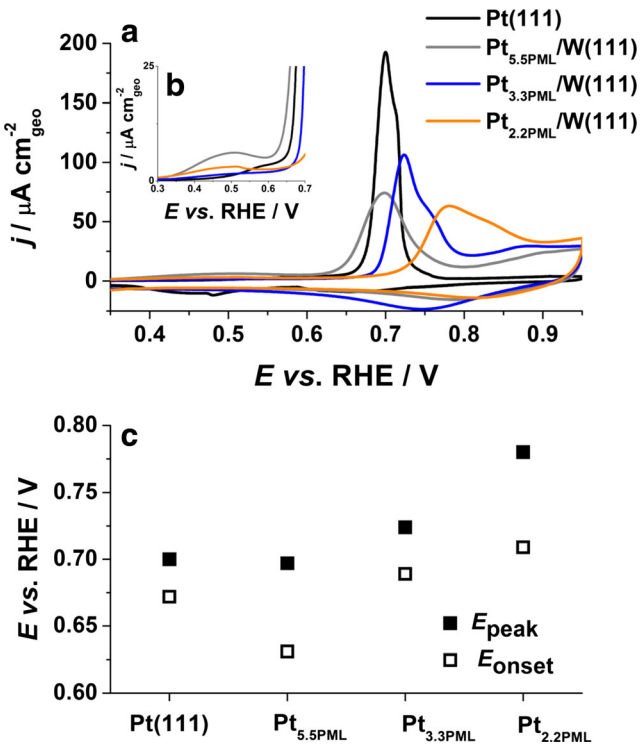

Fig. 7 **a** CO_{ads} stripping voltammograms measured on a W(111) single crystal covered by 2.2, 3.3 or 5.5 physical monolayers of Pt, **b** zoom in the potential region $0.3<E<0.7$ V vs. RHE and **c** potential of the onset and of the CO_{ads} electrooxidation peak. The onset potential was defined as the potential at which 10 % of the current value at the peak potential was reached. 0.1 M H_2SO_4, ν=0.02 V s^{-1}, E_{ads}=0.1 V vs. RHE

Figure 7a shows the CO_{ads} stripping voltammograms recorded on the W(111) surfaces covered with 2.2, 3.3 or 5.5 physical monolayers and that measured on a Pt (111) single crystal for comparison. Similar to what was observed for the adsorption of H_{upd}, the catalytic properties of the Pt_{xPML}/W(111) are markedly different from that of the Pt(111) electrode. Figure 7 shows that both the onset and the main CO_{ads} stripping peak potential shift towards positive potential with decreasing the number of deposited Pt monolayers. This suggests that the coverage with OH_{ads} species required to oxidize the adsorbed CO molecules (Eq. 4) is lowered on the thinner Pt films. The position of the CO_{ads} stripping peak on Pt(111) and $Pt_{5.5PML}$/W(111) is very close—E=0.70 V vs. RHE—thereby suggesting that both surfaces have similar catalytic properties or, in other terms, that strain and ligand effects have vanished at this coverage. Interestingly, we also noticed that a pre-peak developed between E=0.35 and 0.60 V vs. RHE (Fig. 7b) on the $Pt_{2.2PML}$/W(111) and $Pt_{5.5PML}$/W(111) surfaces: This pre-peak was ascribed to the oxidation of CO molecules adsorbed on surface defects (adatoms and step edges) in analogy with former observations on Pt(111) and stepped surfaces in the literature [32–35]. The increased surface reactivity of the thicker Pt films agrees with their highly defective nature in particular with the presence of strain-induced misfit dislocations as discussed in the section "Structural Characterization of the Pt/W(111) Surfaces". The effect of the crystalline orientation, the terrace width and the density of structural defects on the CO_{ads} electrooxidation kinetics has been widely discussed in the work of Lebedeva et al. [32–34]. However, it is believed to have minor influence compared to strain and ligand effects induced by the W(111) substrate.

Finally, we stress that the CO_{ads} stripping peaks become increasingly asymmetric and seem to be composed of multiple peaks when the number of Pt monolayers decreases. This phenomenon may be rationalized by considering that (i) the fraction of active sites where OH species are generated from water splitting is lowered on the most compressed Pt films, (ii) the adsorption of anions or the relaxation of CO islands during CO_{ads} electrooxidation blocks the freed Pt atoms and prevents the dissociative adsorption of water molecules, and/or (iii) different multilayer structures featuring different surface reactivity are present on the thinner Pt films. In the frame of the first hypothesis, we emphasize that the potential difference between the onset and the main CO_{ads} stripping peak potential varies monotonously with the number of deposited Pt monolayers (Fig. 7b), therefore suggesting that OH_{ads} formation is not limiting the reaction kinetics in the potential range investigated. The second hypothesis may also be ruled because the CO_{ads} stripping peak is narrow on Pt(111). In consequence, the pronounced current tailing at high electrode potential (superior to the current maximum) was tentatively ascribed to the presence of different multilayer structures, i.e. Pt adislands featuring different thickness and morphology, in the thinner Pt/W(111) films. Although pieces of evidence of this hypothesis could not be obtained by scanning tunnelling microscopy, it is very well established that Volmer–Weber or 3D growth is favoured during heteroepitaxial metal deposition. In consequence, the surface of the thinner Pt/W(111) films is believed to be composed of Pt adislands with different sizes (number of atoms), height and thus surface reactivity. In that respect, we refer to former work of Kibler et al. [15, 16] in which the polarization curves obtained on Pt monolayers supported onto different single crystals always contained multiple peaks, which were ascribed to different reaction rates on strained and unstrained regions of the Pd films. A last but hardly provable hypothesis would be that CO_{ads} molecules are stabilized on the thinnest Pt films, thereby decreasing the rate of Eq. 5. Keeping the same idea in mind, it is noteworthy that similar tailing and multiple CO_{ads} electrooxidation peaks were observed by Maillard et al. [36–38] on Pt nanoparticles with different sizes and related to restricted CO_{ads} surface mobility. The authors showed that the CO_{ads} diffusion coefficient strongly depends on the nanoparticle size and that a transition towards fast diffusion was observed when the Pt nanoparticle size exceeded ca 3 nm.

Conclusion

In conclusion, Pt atoms were deposited on a W(111) single-crystal electrode via molecular beam epitaxy. A minimal coverage of 2.2 physical monolayers was found necessary to ensure the stability of the Pt/W(111) electrode in acidic electrolyte as shown by combined cyclic voltammetry and XPS experiments. Below this coverage, a certain number of W atoms are exposed to the acidic electrolyte, leading to the formation of WO_3 and inducing the desorption of the Pt films from the W(111) single crystal. Above this coverage, the Pt films were found to be stable in the acidic electrolyte. The chemisorption energy of H_{upd} and OH species on Pt_{xPML}/W(111) strongly depends on the number of deposited Pt physical monolayers as reflected by cyclic voltammograms. The H_{upd} adsorption/desorption region is shifted to lower electrode potential as the number of Pt physical monolayers decreased, in good agreement with the *d*-band theory. More compressed Pt monolayers feature decreased surface reactivity for the electrochemical CO_{ads} oxidation.

Compliance with Ethical Standards

Disclosure of Potential Conflict of Interest The authors declare that they have no conflict of interest (financial or non-financial).

Funding This study was funded by Oseo-Anvar in the framework of the H2E project.

References

1. H.-L. Jiang, Q. Xu, J Mater Chem **21**, 13705 (2011)
2. A.-Q. Wang, C.-M. Chang, C.-Y. Mou, J Phys Chem B **109**, 18860 (2005)
3. R. Parsons, G. Ritzoulis, J Electroanal Chem Interfacial Electrochem **318**, 1 (1991)
4. D.S. Strmcnik, D.V. Tripkovic, D. van der Vliet, K.C. Chang, V. Komanicky, H. You, G. Karapetrov, J. Greeley, V.R. Stamenkovic, N.M. Markovic, J Am Chem Soc **130**, 15332 (2008)
5. W. Yu, M.A. Barteau, J.G. Chen, J Am Chem Soc **133**, 20528 (2011)
6. W.M.H. Sachtler, *Handbook of heterogeneous catalysis, vol. 3* (Wiley-VCH Verlag GmbH & Co. KGaA, Darmstadt, 2008), p. 1585
7. B. Hammer, Y. Morikawa, J.K. Norskov, Phys Rev Lett **76**, 2141 (1996)
8. J.R. Kitchin, J.K. Nørskov, M.A. Barteau, J.G. Chen, J Chem Phys **120**, 10240 (2004)
9. J.R. Kitchin, J.K. Nørskov, M.A. Barteau, J.G. Chen, Phys Rev Lett **93**, 156801 (2004)
10. J.A. Rodriguez, D.W. Goodman, J Phys Chem **95**, 4196 (1991)
11. B. Hammer, J.K. Nørskov, Surf Sci **343**, 211 (1995)
12. A. Ruban, B. Hammer, P. Stoltze, H.L. Skriver, J.K. Nørskov, J Mol Catal A **115**, 421 (1997)
13. I.E.L. Stephens, A.S. Bondarenko, F.J. Perez-Alonso, F. Calle-Vallejo, L. Bech, T.P. Johansson, A.K. Jepsen, R. Frydendal, B.P. Knudsen, J. Rossmeisl, I. Chorkendorff, J Am Chem Soc **133**, 5485 (2011)
14. I.E.L. Stephens, A.S. Bondarenko, U. Grønbjerg, J. Rossmeisl, I. Chorkendorff, Energy Environ Sci **5**, 6744 (2012)
15. L.A. Kibler, A.M. El-Aziz, R. Hoyer, D.M. Kolb, Angew Chem Int Ed **44**, 2080 (2005)
16. L.A. Kibler, A.M. El-Aziz, D.M. Kolb, J Mol Catal A **199**, 57 (2003)
17. M. Gsell, P. Jakob, D. Menzel, Science **280**, 717 (1998)
18. P. Strasser, S. Koh, T. Anniyev, J. Greeley, K. More, C. Yu, Z. Liu, S. Kaya, D. Nordlund, H. Ogasawara, M.F. Toney, A. Nilsson, Nat Chem **2**, 454 (2010)
19. Y. Soldo-Olivier, E. Sibert, B. Previdello, M.C. Lafouresse, F. Maillard, M. De Santis, Electrochim Acta **112**, 905 (2013)
20. H.E. Hoster, O.B. Alves, M.T.M. Koper, Chem Phys Chem **11**, 1518 (2010)
21. M. El-Jawad, J.-L. Chemin, B. Gilles, F. Maillard, Rev Sci Instrum **84**, 064101 (2013)
22. J.W. Matthews, A.E. Blakeslee, J Cryst Growth **27**, 118 (1974)
23. L.B. Freund, S. Suresh, *Thin films materials: stress, defect formation and surface evolution* (Cambridge University Press, Cambridge, 2006)
24. D. Hull, D.J. Bacon, in *Introduction to dislocations*, ed. by D. Hull, D.J. Bacon (Butterworth-Heinemann, Oxford, 2001), p. 82
25. S. Jayaraman, T.F. Jaramillo, S.H. Baeck, E.W. McFarland, J Phys Chem B **109**, 22958 (2005)
26. F. Micoud, F. Maillard, A. Gourgaud, M. Chatenet, Electrochem Commun **11**, 651 (2009)
27. F. Micoud, F. Maillard, A. Bonnefont, N. Job, M. Chatenet, Phys Chem Chem Phys **12**, 1182 (2010)
28. M. Pourbaix, *Atlas d'Equilibres Electrochimiques* (Gauthier-Villars & Cie, Paris, 1963)
29. D.F. Van Der Vliet, C. Wang, D. Li, A.P. Paulikas, J. Greeley, R.B. Rankin, D. Strmcnik, D. Tripkovic, N.M. Markovic, V.R. Stamenkovic, Angew Chem Int Ed **51**, 3139 (2012)
30. C.D. Wagner, W.M. Riggs, L.E. Davis, J.F. Moulder, *Handbook of X-ray photoelectron spectroscopy* (Perkin-Elmer Corp. (Physical Electronics), Eden Prairie, 1979)
31. V. Pallassana, M. Neurock, L.B. Hansen, B. Hammer, J.K. Norskov, Phys Rev B **60**, 6146 (1999)
32. N.P. Lebedeva, M.T.M. Koper, E. Herrero, J.M. Feliu, R.A. van Santen, J Electroanal Chem **487**, 37 (2000)
33. N.P. Lebedeva, A. Rodes, J.M. Feliu, M.T.M. Koper, R.A. van Santen, J Phys Chem B **106**, 9863 (2002)
34. N.P. Lebedeva, M.T.M. Koper, J.M. Feliu, R.A. van Santen, J Phys Chem B **106**, 12938 (2002)
35. A. López-Cudero, A. Cuesta, C. Gutiérrez, J Electroanal Chem **579**, 1 (2005)
36. F. Maillard, M. Eikerling, O.V. Cherstiouk, S. Schreier, E. Savinova, U. Stimming, Faraday Discuss **125**, 357 (2004)
37. F. Maillard, E.R. Savinova, P.A. Simonov, V.I. Zaikovskii, U. Stimming, J Phys Chem B **108**, 17893 (2004)
38. F. Maillard, E.R. Savinova, U. Stimming, J Electroanal Chem **599**, 221 (2007)